Electric control of power extracting end-stop for MEMS vibration energy harvesting

You may also be interested in:

Electric control of power extracting end-stop for MEMS vibration energy harvesting

Binh Duc Truong, Cuong Phu Le and Einar Halvorsen

Department of Micro- and Nanosystem Technology, Buskerud and Vestfold University College, Campus Vestfold, Raveien 215, 3184 Borre, Norway

E-mail: `Einar.Halvorsen@hbv.no`

Abstract. This experimental work investigates a technique to further improve performance of vibration energy harvesters under displacement-constrained operation. Previously, a device concept based on end-stops acting as additional transducers was developed so that the harvested power can be increased beyond the power obtained from a conventional harvester of the same size. However, there is a range of tested acceleration amplitudes in which the transducing end-stop device performs worse than the conventional device. In this paper, an approach using electric control is used to optimize the end-stop transducer performance and thereby further improve the system effectiveness under displacement constrained operation. For example, the maximum power increases by a factor of 2.4 compared to that of a conventional prototype under the same operating conditions and constrained displacement amplitude, while this value was about 1.3 for the previous technique.

1. Introduction

MEMS vibration energy harvesting is a technology to replace batteries in wireless sensor systems and other microscale applications. A harvester converts ambient mechanical energy into electrical energy to power the system. Typically, the energy converter is designed as a spring-mass system and is based on either of three basic mechanisms: piezoelectric, electromagnetic or electrostatic conversion [1–5]. For low loss, resonant microscale devices, the limited space available on chip can limit the proof mass displacement constraining it to a maximum amplitude X_{max}. This limitation has consequences when the vibration is strong enough. Usually, end-stops are designed to reliably define the motion range of the proof mass while preventing structural damage. To provide their function, end-stops tend to be rigid compared to the proof mass suspension. A positive effect of using the rigid end-stops is the ability to enhance system bandwidth seen in several recent works [6,7]. Nevertheless, saturated power is a major limitation observed when the proof mass hits the end-stops. In order to overcome this shortcoming, we previously introduced a device concept that uses active end-stops as additional transducers to extract extra power from internal impacts and thereby adding to the power of the main transducers. The prototypes have demonstrated improved power even when the maximum displacement amplitude is reached [8].

Despite the advantages of the end-stop transducers, there is still an undesirable gap in the tested range of acceleration amplitudes where the impact device has no benefit. A prototype in [9] with reduced mechanical stiffness for the end-stop transducers somewhat reduces this gap.
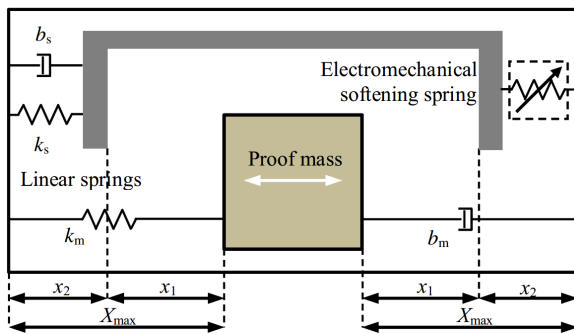
Figure 1. Device concept for utilization of movable end-stop functioning as additional transducer; the main proof mass is constrained to a maximum displacement X_{max} by rigid end-stops
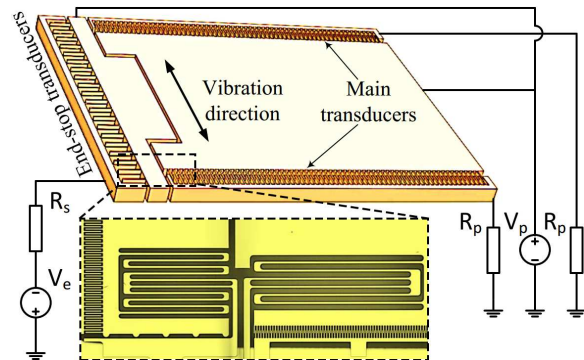
Figure 2. Schematic layout and close-up view of the fabricated impact device including main and end-stop transducers

In this work, an investigation on using electric control to reduce the effective stiffness of the end-stop transducer, and thereby further shrink the acceleration gap, is presented.

2. MEMS impact device and description

Figure 1 illustrates the device concept with the end-stop transducer that is simply represented by a spring-mass-damper system. Under sufficiently large accelerations, the main proof mass repeatedly collides with the end-stop transducer and both transducers contribute power. For small accelerations, there are no impacts and the contribution to output power from the end-stop transducer is negligible. The active area of the prototype is 4×5 mm^2 and is mostly occupied by the main proof mass and its transducer structure. The main proof mass m_m is much larger than the mass of the end-stop structure which is $m_s \sim \frac{m_m}{20}$. The maximum displacement amplitude is $X_{max} = 10$ μm. At equilibrium, the distance between the end-stop proof mass and the main proof mass is $x_1 = 6$ μm and the distance between the end-stop proof mass and the rigid end-stops is $x_2 = X_{max} - x_1 = 4$ μm.

Figure 2 shows the close-up view of the impact device, which is fabricated in the SOIMUMPS process with 25 μm device layer thickness. The main transducer is an ordinary comb-drive structure with two anti-phase overlap varying capacitances and the end-stop transducer is a gap-closing structure. All proof masses are suspended by linear folded-springs. The symmetric gap-closing structure exerts an electrostatic force corresponding to a negative stiffness, which plays a role as an electromechanical softening spring and consequently reduces the net linear stiffness of the end-stop. Further detailed parameters of the impact device can be found in [10].

A bias $V_s = V_p + V_e$ is used to control the end-stop transducer while the main-transducer bias is kept constant at V_p=9 V. When V_s increases, the net linear stiffness of the end-stop transducer decreases due to the electrostatic attraction which corresponds to a negative stiffness. Ultimately the net stiffness goes to zero at a critical value ~ 22 V and a linear instability occurs. At V_s above ~ 15 V, the end-stop transducer tends to dynamically pull in and stick to its own rigid end-stop, so all reported tests were conducted below this value.

In the experiments, output powers are simply measured by connecting the transducers to external resistive loads and measure the voltage across the loads. The voltages are measured through buffer amplifiers and collected by a NI-USB-6211 DAQ controlled by a computer with
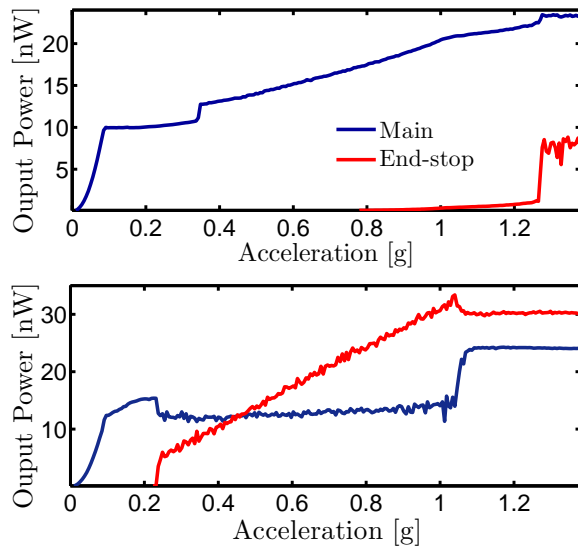
Figure 3. Measured output power of the main and end-stop transducers in sweeps of acceleration amplitude at fixed main bias voltage V_p=9 V and resonant frequency f_0=648.5 Hz for different end-stop bias voltage V_s=9 V (top) and 14.5 V (bottom)
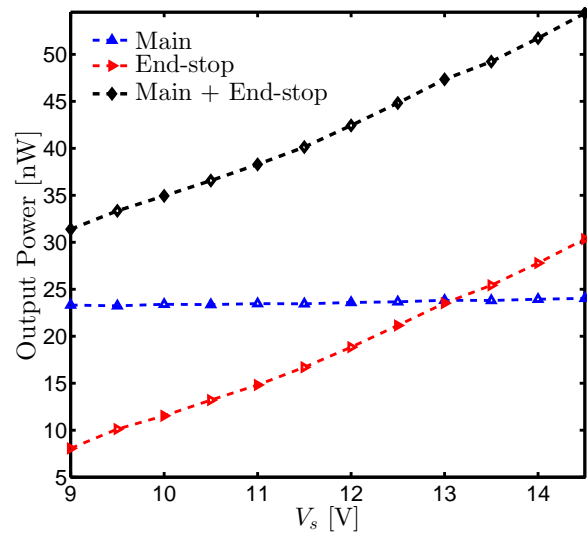
Figure 4. Measured output power of the main and end-stop transducers under increased end-stop bias voltage at fixed main bias voltage V_p=9 V, resonant frequency f_0=648.5 Hz and acceleration A=1.38 g

National Instruments LabView software. A TIRA vibration exciter is used to generate the vibrations. The total power of the impact device is the sum of powers from the main and end-stop transducers.
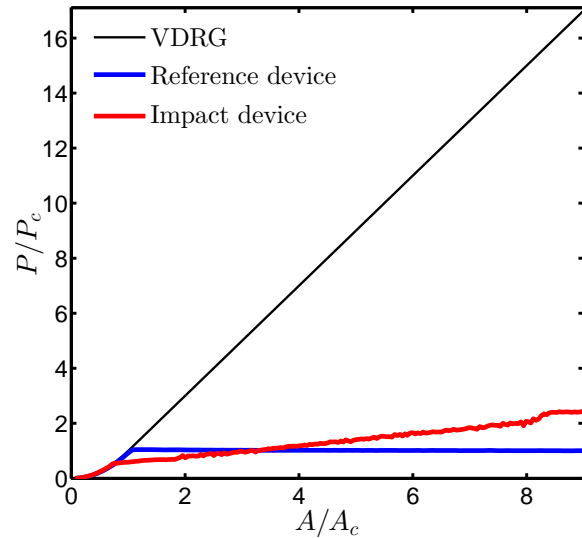
3. Measurements

Figure 3 shows effects of the electric control on output power of the impact device, where output powers of the main and end-stop transducers are measured in acceleration sweeps at resonant frequency f_0=648.5 Hz for different end-stop bias voltages V_s=V_p=9 V and V_s=14.5 V. The measured results indicate that the internal impact starts at an acceleration amplitude A=0.09 g. For $A > 0.09$ g, output power of the main transducers increases roughly linearly before reaching maximum value of P=23.4 nW at A=1.28 g for V_s=9 V, while for V_s=14.5 V a less acceleration amplitude of A=1.04 g is sufficient to obtain maximum power. In addition, the power extracted from the end-stop starts to increase when the acceleration amplitude exceeds A=0.24 g for V_s=14.5 V. This is a significant reduction compared to the value A=1.28 g observed when V_s=9 V. Power contribution from the transducing end-stop for V_s=14.5 V is much better than that for V_s=9 V, for example, about 3.78 times higher at their maximum levels.

Measured output powers of the main and end-stop transducers under increasing V_s are shown in Figure 4. The power extracted from the end-stop transducer is roughly linear in V_s in the impact regime while that of main transducers remains unchanged. However, in order to obtain significant benefits from the transducing end-stop compared to that of the main structure, high bias voltage for the gap-closing transducer is required while still maintain dynamic stability. The output power of end-stop transducer is equal to that of the main transducer at V_s=13 V giving P=23.8 nW and even higher for further increase provided $V_s < V_{pull-in}$.

In order to validate the technique for power improvement, the impact device performance is compared to that of a conventional reference device with rigid end-stops. The reference device is
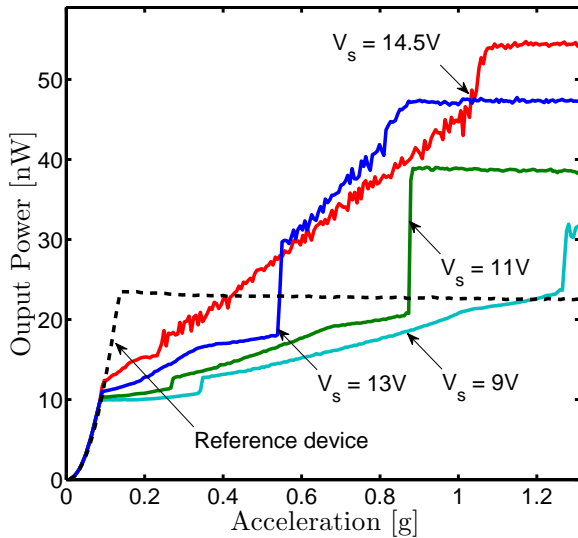
Figure 5. Measured total output power of the impact and reference devices at their resonant frequencies with different values of end-stop bias voltage. The bias is V_p=9 V for both main transducer and for reference device

Figure 6. Measured total output power of the impact and reference devices compared to optimal velocity-damped generator VDRG

designed to have the same active area and the same maximum displacement amplitude X_{max}=10 μm as the impact device. Thus, the reference device is similar to the main transducer part of the impact device, but has space for bigger mass and larger transducers. The reference transducers are biased by the same voltage V_r=V_p=9 V. The total power of both devices at their resonant frequencies are shown in Figure 5. The conventional device displays saturated power P=23.8 nW when X=X_{max} at A=0.14 g. When increasing V_s from 9 V to 14.5 V, the output power is growing almost linearly before reaching the saturation power, instead of exhibiting jump phenomena as observed for lower bias voltages. The power of the impact device is equal to that of reference device at A =1.2 g for V_s=9 V, but this critical acceleration decreases from A =0.9 g, 0.5 g to 0.4 g when increasing from V_s=11 V, 13 V to 14.5 V respectively. Hence, the undesirable gap in the beneficial range of acceleration amplitudes for the impact device is reduced from 1.1 g to 0.3 g when V_s =14.5 V, making the impact technique useful at a significantly lower acceleration. For $A > 1.05$ g, the total power of impact device is 2.4 times higher than that of the reference device.

4. Discussion

The two devices are compared to the optimal velocity-damped generator (VDRG) which has nearly the maximum possible power [11] as shown in Figure 6. The output power and the input acceleration are normalized respectively by the factors P_c=$2\pi^2 f_0^2 X_{max}^2 b_r$ and A_c=$\frac{4\pi f_0 X_{max} b_r}{m_r}$ where m_r is the proof mass of the reference device and b_r is the mechanical damping of the reference device found from fit to measurement in the linear regime. The comparison demonstrates that even though the end-stop transducer is advantageous in enhancing the power under displacement-constrained operation, the obtained power is considerably lower than the maximum possible. It is interesting to consider approaches that could further boost power in the impact regime. It seems unavoidable to consider the more complicated approach of load

optimization that tracks the acceleration amplitude, which is what the VDRG result corresponds to. One could also expect benefits from further developed design of the end-stop transducer, for example by combining a mechanical hardening spring with electromechanical softening while keeping the system stability in order to achieve low stiffness and high electrical damping.

5. Conclusion

A method using the electric control of the end-stop transducer has improved the performance of the impact device comparing to previous techniques in [9,10] that caused lower power and jump phenomenon. Separate tuning the bias V_s of the end-stop transducer is able to drive its effective stiffness extremely low thanks to the attractive electrostatic force. The transducing end-stop therefore actively extracts more power from the internal impact at even lower force amplitude than the previous design. The technique displays reduction of the undesirable acceleration gap and increase of the maximum power. Nevertheless, it is clear that despite the improvements, there is still considerable room for improvement before the fundamental physical limit is reached in future works.

Acknowledgment

References

[1] Mitcheson P D, Yeatman E M, Rao G K, et al. (2008) *Proc. of the IEEE* **96** 1457–1486
[2] Roundy S, Wright P K and Rabaey J M (2003) *Computer Communication* **26** 1131–1144
[3] Roundy S, Wright P K and Rabaey J M (2004b), London: Kluwer Academic Publishers. ISBN: 1–4020–7663–0
[4] Moss S, Barry A, Powlesland I, Galea S and Carman G P, 2011 *Smart Mater. Struct.* **20** 045013
[5] Lei Gu and Carol Livermore, 2011 *Smart Mater. Struct.* **20** 045004
[6] Hoffmann D, Folkmer B and Manoli Y, 2009 *J. Micromech. Microeng.* **19** 094001
[7] Soliman M S M, Abdel-Rahman E M, El-Saadany E F and Mansour R R, *J. Micromech. Microeng.*, **18** (2008) 115021
[8] Le C P, Halvorsen E, Søråsen O and Yeatman E M, *J. of Int. Mat. Syst. Struc.*, **23** 1409–21
[9] Le C P, Halvorsen E, Søråsen O and Yeatman E M, *Proc. PowerMEMS* 2012: 444–7
[10] Le C P, Halvorsen E, Søråsen O and Yeatman E M, *Proc. PowerMEMS* 2011: 122–5
[11] Halvorsen E, Le C P, Mitcheson P D and Yeatman E M, 2013 *J. Phys.: Conf. Ser.* **476** 012026